Magneto-optical Kerr switching properties of $(CrI_3)_2$ and $(CrBr_3/CrI_3)$ bilayers

Ke Yang,[†] Wentao Hu,[†] Hua Wu,[*,†,‡] Myung-Hwan Whangbo,[¶,§,‖] Paolo G. Radaelli,[⊥] and Alessandro Stroppa[*,#]

†*Laboratory for Computational Physical Sciences (MOE), State Key Laboratory of Surface Physics, and Department of Physics, Fudan University, Shanghai 200433, China*

‡*Collaborative Innovation Center of Advanced Microstructures, Nanjing 210093, China*

¶ *Department of Chemistry, North Carolina State University, Raleigh, North Carolina 27695-8204, USA*

§ *State Key Laboratory of Crystal Materials, Shandong University, Jinan 250100, China*

‖*State Key Laboratory of Structural Chemistry, Fujian Institute of Research on the Structure of Matter, Chinese Academy of Sciences, Fuzhou, Fujian 350002, China*

⊥*Clarendon Laboratory, Department of Physics, University of Oxford,Parks Road, Oxford OX1 3PU, United Kingdom*

#*CNR-SPIN, c/o Dip.to di Scienze Fisiche e Chimiche -Università degli Studi dell'Aquila - Via Vetoio - 67100 - Coppito (AQ), Italy*

E-mail: wuh@fudan.edu.cn; alessandro.stroppa@spin.cnr.it

Abstract

Abstract: We explore the magneto-optical Kerr effect (MOKE) for different spin configurations of $(CrI_3)_2$ bilayer and $(CrBr_3/CrI_3)$ mixed bilayer, using symmetry arguments and first-principles electronic structure calculations. Starting from CrX_3 (X = I, Br) monolayers, we considered collinear ferromagnetic (FM) and layered antiferromagnetic (AFM) states for $(CrI_3)_2$ and $(CrBr_3/CrI_3)$ bilayers. The AFM $(CrI_3)_2$ bilayer does not show MOKE, consistent with the presence of a symmetry operator combining inversion (I) and time reversal (T) symmetries. The FM state preserves I symmetry but breaks the T symmetry, thus allowing a non-zero Kerr angle, which is reversible by switching the FM spins. The $(CrBr_3/CrI_3)$ bilayer breaks both the I and T symmetries and thus exhibits MOKE both in the FM and, remarkably, in AFM states. In both FM and AFM configurations, the Kerr angle switches by reversing the spins in both layers. Our study demonstrates that MOKE spectra can help characterize different magnetic configurations in these emerging two-dimensional (2D) materials due to a different stacking of the monolayers, even in the AFM case. Note that the present symmetry analyses and MOKE properties apply to more general 2D magnetic van der Waals heterostructures. Furthermore, we propose $(CrBr_3/CrI_3)$ bilayer as a promising candidate for AFM spintronics, since the two time-reversed AFM states are associated with opposite Kerr rotation, *i.e.* they could be used as memory elements.

Keywords: Two-dimensional magnetic materials, Kerr effect, density functional theory calculations, magnetic symmetry, spin-orbit and spin-texture, switching properties, antiferromagnetic spintronics

1 Introduction

Starting from the experimental demonstration of intrinsic ferromagnetism (FM) in CrI_3 monolayer[1] and $Cr_2Ge_2Te_6$ atomic layers,[2] there has been very significant interest in two-dimensional (2D) magnets.[3–6] The CrI_3[1] and $CrBr_3$[7] monolayers have been successfully

exfoliated from their respective bulk crystals. Experimentally, magneto-optical Kerr effect (MOKE) microscopy studies have demonstrated that CrI_3 monolayer and $Cr_2Ge_2Te_6$ atomic layers show an Ising-like FM behaviour with out-of-plane spin orientation.[1,2,8] This immediately prompted extensive investigations on 2D magnets. For example, the $CrBr_3$ monolayer is isostructural and isoelectronic with CrI_3 and also shows an Ising-like FM behaviour with spin orientation perpendicular to the layer.[7] $CrCl_3$ has also been proposed as new FM monolayer.[9–11]

Bilayers have also been studied, since they show intriguing properties.[8,12–14] The recently synthesized $(CrI_3)_2$ bilayer[8,15] is particularly interesting, since it is a 2D layered antiferromagnet with Neel temperature $T_N = 45$ K and undergoes a reversible transition between AFM and FM states with magnetization that is linearly dependent on the external electric field.[8,12,15] Several explanations have been proposed for the bilayer antiferromagnetism.[13,14,16] Theoretical studies suggest an intriguing connection between the stacking order and the magnetic properties of $(CrI_3)_2$ bilayer such that it is possible to tune the ground-state magnetic order by varying the interlayer stacking order. This would justify the observed AFM ordering in $(CrI_3)_2$ bilayer[12] and may have direct implications on heterostructures made of 2D magnets.[17] Indeed, the appearance of 2D magnets has boosted the study of a wide range of new van der Waals heterostructures (vdWHs) whose syntheses have now become possible, offering new perspectives in this rapidly expanding field where the potential of technological impact is enormous.[18] In fact, exploiting the novel properties of these vdWHs with diverse layering of metals, semiconductors or insulators, ferrelelectric or magnetic materials, new designs of electronic devices emerge, including tunnelling transistors, barristors and flexible electronics, as well as optoelectronic devices, including photodetectors, photovoltaics and light-emitting devices with unprecedented characteristics or unique functionalities.

Antiferromagnets are attractive for spintronic applications because they have zero net moment, thus exhibiting several advantages over ferromagnets for memory device applications: insensitivity to external magnetic fields, much faster spin dynamics (THz) and higher

packing density due to the absence of any stray field.[19–21] Methods to achieve reversal of AFM moments and detect them by electrical or optical means have attracted great attention.[22–24] For example, it was recently demonstrated that the spins can be reversed in a collinear AFM CuMnAs thin film and can be electrically distinguished by measuring a second-order magnetoresistance effect.[22] Furthermore, the control of magnetism by the application of small gate voltages in field-effect devices was demonstrated in CrI_3 bilayer, showing their potential applications in AFM spintronics.[8,12]

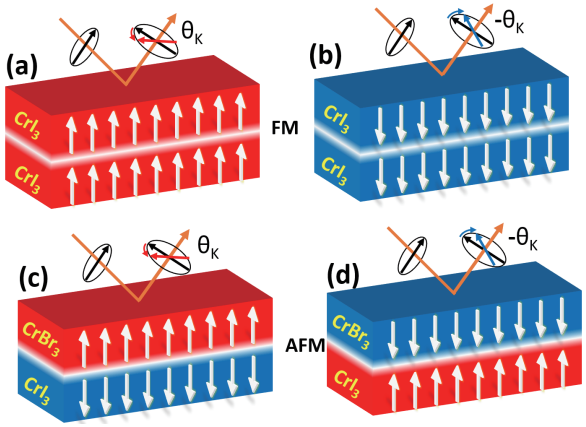

Figure 1: Schematic diagram of MOKE and its switching upon reversal of the magnetization in (a) up-up (u-u), (b) down-down (d-d) FM states of $(CrI_3)_2$ bilayer and (c) up-down (u-d), (d) down-up (d-u) AFM states of $(CrBr_3/CrI_3)$ bilayer.

For a variety of magnetic systems, MOKE has been extensively employed as a very sensitive probe of electronic structure, exchange coupling, magnetic anisotropy and lattice symmetry breaking.[25,26] The presence or absence of a MOKE signal depends on the magnetic symmetry of the material under investigation (Here, we assume the relevant tensor to be the antisymmetric part of the dielectric (or impermeability) tensor, which is defined in the Bilbao Crystallographic Server as the spontaneous Faraday tensor[27]). More specifically, Neumann's principle[28] prescribes that when the point group of the material contains either the time reversal symmetry operator (T) or the time reversal combined with inversion (TI), there is no MOKE in the system. Thus, a magnetic material can become magneto-optically active when both the T and TI symmetries are broken in the point group. In most com-

mensurate magnetic structures, the T symmetry is lost in the point group when magnetic ordering (*e.g.*, an AFM or FM ordering) takes place, while, in many cases, the TI symmetry survives. This opens up the possibility to *turn on* magneto-optical effects by breaking spatial inversion, since breaking inversion (I) symmetry automatically results in breaking TI symmetry, provided that T is already broken. For 2D systems, this can be achieved by breaking the mirror reflection symmetry M_z or the in-plane inversion symmetry C_2, as confirmed by some theoretical and experimental reports.[29–31]

In this work, we study the MOKE $(CrI_3)_2$ and $(CrBr_3/CrI_3)$ bilayers where the spins have a FM configuration with an out-of plane magnetic anisotropy in each CrX_3 (X = I, Br) monolayer, see Figure 1. Each CrX_3 (X = I, Br) monolayer consists of edge-sharing CrX_6 octahedra, which form a honeycomb lattice of Cr^{3+} ions, see the inset of Figure 2. In the $(CrBr_3/CrI_3)$ mixed bilayer, both the T and the M_z symmetries are broken due, respectively, to the FM order in each monolayer and the presence of two chemically distinct monolayers. Using symmetry analyses and first-principles calculations, we show that $(CrBr_3/CrI_3)$ bilayer exhibits MOKE not only in the FM but also in the AFM arrangement between the two FM layers. Interestingly, the MOKE can be switched by spin reversal in the AFM $(CrBr_3/CrI_3)$ bilayer — an appealing effect for AFM spintronics since the two time-reversed AFM states of the mixed bilayer are associated with opposite Kerr rotation. Recently, there has been an increasing interest in antiferromagnets as prospective spintronic materials for high-density and ultrafast memory devices, owing to their vanishingly small stray field and orders-of-magnitude faster spin dynamics compared to their FM counterparts. In our case, the two AFM states (up-down vs down-up) are associated with two different Kerr signals, and, therefore, could be treated as two distinct "information states" (bits '0' or '1') to be read magneto-optically. Further experimental work is required to engineer and exploit these effects in practical devices.

2 Symmetry Considerations

The spontaneous Kerr rotation effect (hereafter referred to as MOKE) depends upon the incident photon energy hν and it arises from a combined action of spin-orbit coupling (SOC) and non-zero spin polarization.[32–34] In high-symmetry situations and near-normal incidence,[33] this effect can be fully described by a complex angle defined as:

$$\phi_K = \theta_K + \mathrm{i}\eta_K = \frac{-\sigma_{xy}}{\sigma_{xx}\sqrt{1 + \left(\frac{4\pi i}{\omega}\right)\sigma_{xx}}} \tag{1}$$

where σ_{xx} and σ_{xy} are the diagonal and off-diagonal elements of the optical conductivity tensor, respectively, and the real (θ_K) and imaginary (η_K) parts correspond to Kerr angle (rotation of the major axis in the reflected light relative to the polarization axis of the incident light) and ellipticity (a phase difference between the electric-field components perpendicular and parallel to the plane of the reflected light), respectively. Equation (1) usually applies to bulk systems as obtained from the volume dependence of Kubo's formula (see Supporting Information). In our DFT calculations, a slab model with the same thickness was used to simulate both $(CrI_3)_2$ and $(CrBr_3/CrI_3)$ bilayers. While the absolute values of the Kerr rotations may depend on the specific details of the formulation depending on the actual value of thickness, the switching properties do not depend on these details. Furthermore, the relative values of the Kerr rotations and particularly their signs, when comparing different magnetic states, are robust with respect to the specific formula used in the calculations since they are supported by symmetry considerations. More generally, the numerator of Equation (1) is the *antisymmetric* part of the optical conductivity, which is a time-reversal-odd, polar (*i.e.* parity-even) tensor of rank 2. There is a well-known mutual relation between a generic tensor A_{ij} having this symmetry and a time-reversal-odd axial vector m_i, expressed by the relations: $A_{ij} = \varepsilon_{ijk}m_k$, $m_i = \frac{1}{2}\varepsilon_{ijk}A_{jk}$. Since the axial vector m_i has the transformation properties of a magnetic moment; it follows, therefore, that in order for MOKE to be allowed, the magnetic point group of the material should be one of the 31 pyromagnetic point

groups (see Supporting Information) (1, –1, 2, 2′, m, m′, 2/m, 2′/m′, 2′2′2, m′m2′, m′m′2, m′m′m, 4, –4, 4/m, 42′2′, 4m′m′, –42′m′, 4/mm′m′, 3, –3, 32′, 3m′, –3m′, 6, –6, 6/m, 62′2′, 6m′m′, –6m′2′,6/mm′m′), and it should allow for a FM moment, which can, however, be vanishingly small — in other words, MOKE can in principle arise in a fully compensated AFM system.[29,30,35,36] The intriguing possibility of tuning and switching the Kerr angle in AFM compounds have been discussed in the context of multiferroic hybrid perovskites[37] and other systems upon application of external electric fields.[8,12,29–31] However, the switching of MOKE by reversal of spins in a 2D AFM material is highlighted in this work. We believe that this effect could be exploited in memory elements.

One of the necessary (but not sufficient) conditions for MOKE to be allowed is that the magnetic point group should contain neither the T nor the combination TI of time reversal and spatial inversion. Since the MOKE tensor is time-reversal-odd, the MOKE angle will be reversed by reversing all the spin directions. There exists a wide class of centrosymmetric antiferromagnets, of which Cr_2O_3 is the archetype, in which MOKE is forbidden since the point group contains the combination TI symmetry, although T symmetry is broken by magnetic order. This is to be contrasted with the room-temperature magnetic phase of isostructural α-Fe_2O_3, which is weakly FM and therefore MOKE-active, although the FM moment is very small (Note that in the LT phase of α-Fe_2O_3, having point group –3m (vs –3'/m' for Cr_2O_3), is neither weakly FM nor MOKE-active, in spite of the fact that the point group contains neither T not TI. The RT phase of α-Fe_2O_3 has magnetic symmetry 2/m (pyromagnetic).). Only very recently, MOKE research has been extended to collinear and non-collinear antiferromagnets where TI symmetry can be broken by an external electric field.[29–31,37] More generally, systems that are magneto-optically active and predominantly AFM are of great interest for applications in AFM spintronics, particularly if their magnetic symmetry also contains a higher-order axis, which greatly reduces the number of possible domains, and if their magnetic state can be manipulated, *e.g.* by external electric/magnetic fields. This is precisely the case that we will discuss in the remainder.

In the AFM/FM phases of the 2D $(CrI_3)_2$ and $(CrBr_3/CrI_3)$ bilayers, the spins of the two layers are antiparallel/parallel, respectively, with the formal Cr^{3+} S = 3/2. In all cases, there are always two energetically degenerate FM or AFM arrangements, which are related to each other by reversal of all spin directions (equivalent to time reversal for classical spins). Therefore, for example, the up-down and down-up AFM arrangements form a time reversal pair, and so do the up-up and down-down FM arrangements (see Figure 1). For $(CrI_3)_2$ bilayer, the two monolayers are related by crystallographic inversion symmetry, so the net magnetic moment of the AFM phase is exactly zero (without external field), while this is not the case for $(CrBr_3/CrI_3)$ bilayer. However, based on our GGA+U+SOC results (see below), the total magnetic moment for AFM $(CrBr_3/CrI_3)$ bilayer is only 0.003 μ_B/Cr, so the system is effectively a compensated AFM.

To describe all the relevant magnetic states, we introduce two magnetic order parameters $\overrightarrow{L}=\overrightarrow{M_1}-\overrightarrow{M_2}$ (AFM order parameter) and $\overrightarrow{M}=\overrightarrow{M_1}+\overrightarrow{M_2}$ (FM order parameter), where the labels 1 and 2 correspond to top and bottom layers and $|\overrightarrow{M}_{1,2}|$ is the magnetization in the layer, corresponding to a the spin quantum number S = $\pm$3/2 for the Cr^{3+} ions. $\overrightarrow{L}$ distinguishes between the two AFM configurations — up-down (u-d) has $\overrightarrow{L}$ along the *positive* z direction and down-up (d-u) along the *negative* z direction — while $\overrightarrow{M}$ distinguishes between the two FM configurations, *i.e.* up-up (u-u) and (d-d). In Section 3, a general magnetic state of the bilayer will be described using the notation ($\pm$L,$\pm$M), where, for example, (+L,0) corresponds to an AFM state with $\overrightarrow{L}$ along the *positive* z direction, etc.

The transformation properties of these vectors upon application of the inversion operator (I), the time reversal operator (T) and combinations thereof are: $I[\overrightarrow{L}] = T[\overrightarrow{L}] = -\overrightarrow{L}$; $TI[\overrightarrow{L}] = \overrightarrow{L}$; $I[\overrightarrow{M}] = \overrightarrow{M}$; $T[\overrightarrow{M}] = TI[\overrightarrow{M}] = -\overrightarrow{M}$. It follows that $\overrightarrow{L}$ is identically zero by symmetry in the presence of symmetry operators I or T, while it is allowed by the combination TI symmetry. Likewise, $\overrightarrow{M}$ is identically zero the presence of symmetry operators T or TI while it is allowed in the presence of I symmetry.

We now consider the magnetic point group symmetry of the bilayers in the different states.

The paramagnetic point groups of $(CrI_3)_2$ bilayer in the RT (Room-Temperature)/LT (Low-Temperature) phases are $2/m1'$ and $-31'$, respectively.[38] These point groups contain both T and I as independent symmetry operators, so $\overrightarrow{L} = \overrightarrow{M} = 0$, as expected. The corresponding magnetic point groups for the AFM state are $2/m'$ and $-3'$ (non-pyromagnetic and therefore non-MOKE-active). Neither of these groups contains either I symmetry or T symmetry as separate operators, but they both contain the combination TI symmetry, so $\overrightarrow{L} \neq 0$ and $\overrightarrow{M} = 0$. The point groups in the FM state are $2/m$ and -3 (both pyromagnetic/Moke-active groups, as required), both containing I but not T, so that $\overrightarrow{L} = 0$ and $\overrightarrow{M} \neq 0$, again, as expected.

For $(CrBr_3/CrI_3)$ bilayer, the mirror plane and inversion (for RT/LT phases, respectively) are lost, so the corresponding paramagnetic groups are $21'$ and $31'$, while the magnetic groups are 2 and 3 in both AFM and FM states. Since 2 and 3 are both pyromagnetic groups and neither contains I symmetry or T symmetry, the expectation from our symmetry analysis is that $(CrBr_3/CrI_3)$ should be MOKE-active in both FM and AFM states, and that $\overrightarrow{L} \neq 0$, $\overrightarrow{M} \neq 0$ in both cases.

These results are confirmed by an analysis of the symmetry-adapted forms of the relevant conductivity tensors, performed using the MTENSOR software in the Bilbao Crystallographic Server.[39] Here, we focus on the ground state LT structures, which all have point groups containing a three-fold axis, and are relevant for our first-principles calculations (see Section 3). As already stated (see Equation (1)), a non-zero MOKE effect is signalled by the appearance of antisymmetric, off-diagonal terms σ_{xy} in the conductivity tensor in the magnetic state.[33,34] For a solid with at least three-fold rotational symmetry, the general form of the optical conductivity tensor is:

$$\begin{pmatrix} \sigma_{xx} & \sigma_{xy} & 0 \\ -\sigma_{xy} & \sigma_{xx} & 0 \\ 0 & 0 & \sigma_{zz} \end{pmatrix}$$

which is also the general form for FM $(CrI_3)_2$ (point group -3) and FM/AFM ($CrBr_3$/CrI_3) (point group 3). As for the paramagnetic phases (point group $-31'$ or $31'$) and AFM $(CrI_3)_2$ (point group $-3'$), $\sigma_{xy} = \sigma_{yx} = 0$ so that the general form of the tensor is:

$$\begin{pmatrix} \sigma_{xx} & 0 & 0 \\ 0 & \sigma_{xx} & 0 \\ 0 & 0 & \sigma_{zz} \end{pmatrix}$$

Although Equation (1) does not hold for the RT monoclinic phases of $(CrI_3)_2$ bilayer, one can apply the same analysis, and show that the off-diagonal elements of the antisymmetrized conductivity tensor are zero by symmetry for the paramagnetic and AFM phases (point groups 2/m1', 2/m', respectively), while they are allowed to be non-zero for the FM phase (point group 2/m). Consistent with our earlier discussion, MOKE is only allowed in the FM phase, as expected.

Methods

$(CrI_3)_2$ and ($CrBr_3$/CrI_3) bilayers, both in the AB stacking mode of LT CrI_3 bulk, were optimized using the Vienna Ab-initio Simulation Package (VASP),[40] based on the projector augmented wave method and the generalized gradient approximation with the PBE functional.[41,42] To account for the electron correlation of the Cr $3d$ states, the Hubbard U = 3.0 eV and Hund exchange J_H = 0.9 eV with the Liechtenstein linear response approach were included in our calculations.[43,44] The optimized lattice constant of the $(CrI_3)_2$ bilayer $a = b = 6.99$ Å is close to (within 2%) the experimental $a = b = 6.87$ Å of the CrI_3 bulk.[38] Naturally, the optimized ($CrBr_3$/CrI_3) bilayer has a little smaller $a = b = 6.66$ Å, and its dynamical stability is verified by phonon calculation[45] (see the inset of Figure 3). The compressive (tensile) strain for CrI_3 ($CrBr_3$) layer in the ($CrBr_3$/CrI_3) bilayer does not alter the relatively robust intralayer FM coupling, but could tune the subtle interlayer FM

or AFM coupling. Analysis of such a consequence and its effect on the MOKE signals is the primary concern of the present work. Then, to calculate the MOKE, the *exciting* code[46] was used with the (linearized) augmented plane waves plus a local orbitals [(L)APW+lo] basis.[47] The muffin-tin radii for Cr, I and Br atoms are 2.1, 1.8 and 1.8 Bohr, respectively. The (L)APW+lo basis size is determined by $R_{MT}G_{Max} = 5$. The first Brillouin Zone was sampled by a set of 5×5×1 k-points. The SOC is included by the second-variational method. The rotation of the polarization plane, the so-called Kerr rotation θ_K as a function of hν was calculated using time-dependent density-functional theory calculations.[48]

3 First-principles calculations and Discussion

Here we study the MOKE of $(CrI_3)_2$ and $(CrBr_3/CrI_3)$ bilayers using first-principles calculations. For the MOKE calculations, we assume that the light impinges on the top layer in polar MOKE geometry, *i.e.* magnetization direction out of plane and incident light at near normal incidence for which the Equation (1) holds.[33] For both $(CrI_3)_2$ and $(CrBr_3/CrI_3)$ bilayers, the intralayer coupling favors FM, while the interlayer coupling is very subtle and sensitive to the different stacking of the monolayers, with the FM and AFM configurations being very close in energy.[13,14,16] We demonstrate below that the bilayers in the FM or AFM state produce very different MOKE spectra. Therefore, the MOKE spectra can help to identify the different magnetic states and the related stacking mode of the bilayers.

Figure 2 shows the Kerr spectra, *i.e.*, Kerr rotation angles θ_K for the up-up (0, +M), down-down (0, –M), up-down (+L, 0), and down-up (–L, 0) states of the $(CrI_3)_2$ bilayer (see Section 2 for the notations). For the layered AFM states (+L, 0) and (–L, 0), the MOKE spectrum is constantly zero, confirming the symmetry analysis in Section 2. In sharp contrast, the FM (0, +M) and (0, –M) states exhibit non-zero Kerr signals, which is in line with our symmetry considerations and in agreement with experiments.[1,8] The MOKE in $(CrI_3)_2$ bilayer has been studied both in the FM and AFM states experimentally.[1,8] Either

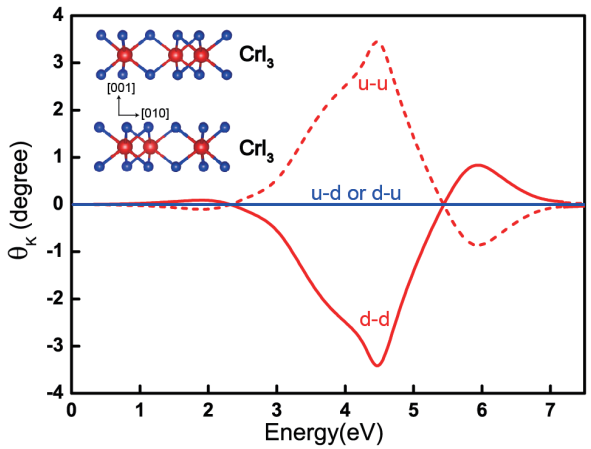

Figure 2: Kerr rotation angle θ_K in the up-up (u-u), down-down (d-d), up-down (u-d), and down-up (d-u) states of $(CrI_3)_2$ bilayer as a function of the incident photon energy hν.

the external magnetic or electric field can be used to switch between FM and AFM state. More specifically, the MOKE of $(CrI_3)_2$ bilayer in the u-u and d-d FM states are opposite in sign while in the u-d and d-u AFM states it is zero in the absence of external fields.[1,8] However, in this work, we describe a mixed ($CrBr_3$/CrI_3) bilayer and demonstrate that its AFM states are magneto-optically active even without external fields. Note that at any given hν , the θ_K values of the (0, +M) and (0, –M) states are opposite in sign, fully in agreement with the well-known fact that the Kerr angle of an FM material can be switched in sign by reversing its magnetization.

Based on above symmetry considerations, we would predict that ($CrBr_3$/CrI_3) bilayer should exhibit MOKE even for (±L, 0) AFM states, because the absence of inversion/mirror symmetry in the structural point group effectively lowers the magnetic symmetry to a pyro-magnetic group. This surprising prediction is now confirmed by our calculations (see Figure 3): while the MOKEs for the (0, +M) and (0, –M) FM states of ($CrBr_3$/CrI_3) bilayer are very similar to the $(CrI_3)_2$ bilayer in the FM states, both the (+L, 0) and (–L, 0) AFM states of ($CrBr_3$/CrI_3) exhibit MOKE, although their spectral intensity is much reduced (one order of magnitude weaker) from the FM states of ($CrBr_3$/CrI_3). This is in striking contrast with the case of the AFM $(CrI_3)_2$ bilayer (no MOKE at all). Moreover, at a given hν, the θ_K value

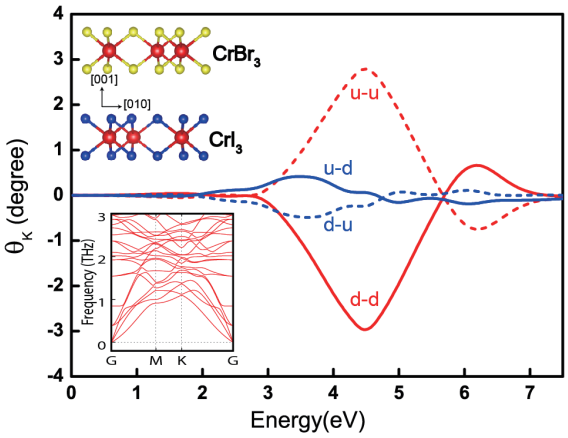

Figure 3: Kerr spectra of the ($CrBr_3$/CrI_3) bilayer in the up-up (u-u) and down-down (d-d) FM states, and in the up-down (u-d) and down-up (d-u) AFM states. The inset shows the phonon spectrum.

of the (+L, 0) AFM state of ($CrBr_3$/CrI_3) is opposite in sign to that of (–L, 0) AFM state, consistent with the time-reversal-odd properties of the MOKE tensor. As noted above, in the ($CrBr_3$/CrI_3) the AFM state may have in principle a non-zero magnetic moment, but in our calculations the net magnetic moment is *practically zero*, being only 0.003 μ_B/Cr. The presence of a MOKE signal in an effectively compensated AFM and, in particular, its reversal upon the change of the AFM states from (+L, 0) to (–L, 0) are indeed surprising and have, to our knowledge, little precedence in the literature. This will be further elucidated below with aid of the calculated band structures and the illustrative energy level diagrams.

Figure 4(a) shows the insulating band structure of the FM (0, +M) $(CrI_3)_2$ bilayer (the band structure for (0, –M) is identical). The valence bands originate mainly from I $5p$ orbitals, while the conduction bands are predominatly from Cr $3d$-e_g orbitals mixed with I $5s5p$. Taking into account the selection rules associated with the Kerr spectral excitation (see Supplemental Materials), we choose to discuss the I $5p \rightarrow 6s$ (or I $5p \rightarrow$Cr e_g) excitation for simplicity. We mark two topmost valence bands with the index 1 and 2, which are characterized by I $5p_x$ and $5p_y$. With the SOC, the combined $\hat{p}_x \pm i\hat{p}_y$ states give rise to the $|l{=}1, l_z{=}\pm 1\rangle$ states depicted in Figure 4(f), while the nearly degenerate bands 1 and 2 arise from the I $5p$ up-spin $|1, +1\rangle$ state in the two CrI_3 monolayers, respectively. This state

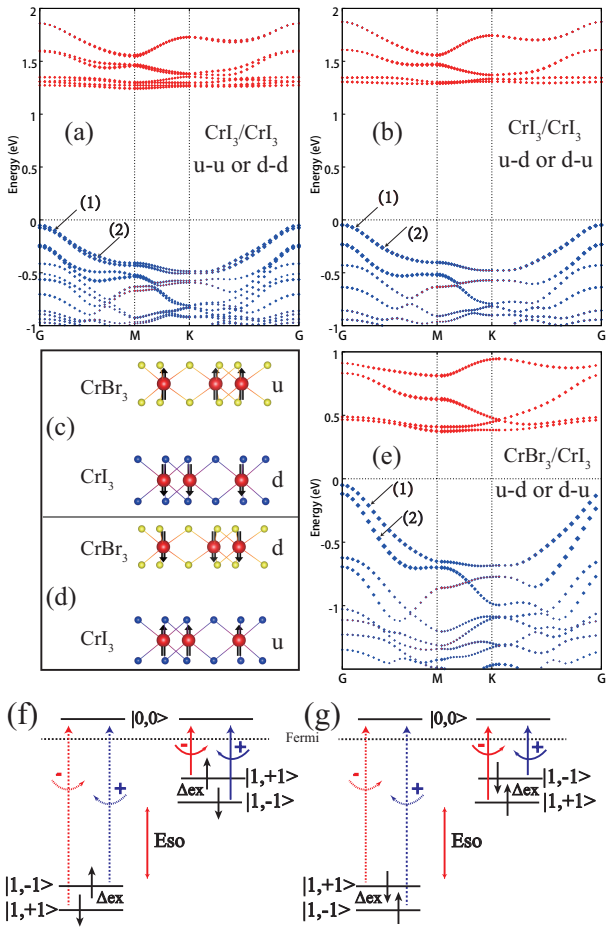

Figure 4: The GGA+U+SOC calculated band structures for (a) the up-up (u-u) or down-down (d-d) FM of $(CrI_3)_2$ bilayer and (b) its up-down (u-d) or down-up (d-u) AFM state, and for (e) AFM ($CrBr_3/CrI_3$) bilayer with (c) up-down (u-d) or (d) down-up (d-u) magnetic structure. The blue curves stand for I $5p_x$ and p_y states, and the red curves the Cr $3d$-e_g orbitals. Fermi level is set at zero energy. The illustrative energy level diagrams (with SOC and exchange splittings) and the excitation spectrum of I $5p \rightarrow 6s$ (Br $4p \rightarrow 5s$) in the FM CrI_3 ($CrBr_3$) monolayer with (f) spin orientation 'up' and (g) 'down' (the – (+) with red (blue) color stands for the absorption of circularly right (left) polarized light).

is separated by a small exchange splitting from the down-spin $|1,-1\rangle$ state, and these two states are separated by a large SOC splitting from the up-spin $|1,-1\rangle$ and down-spin $|1,+1\rangle$ states, see Figure 4(f). Owing to the large SOC of I $5p$ and its negative spin polarization (induced by the strong hybridization with the Cr 3d which has the positive spin=3/2), the down-spin $|1,+1\rangle$ state lies lowest among the four states, and the up-spin $|1,+1\rangle$ state lies highest which gives rise to band 1 for one monolayer (and to band 2 for the other monolayer). These two bands are further elucidated by a spin texture plot shown in Figure 5(a). Then,

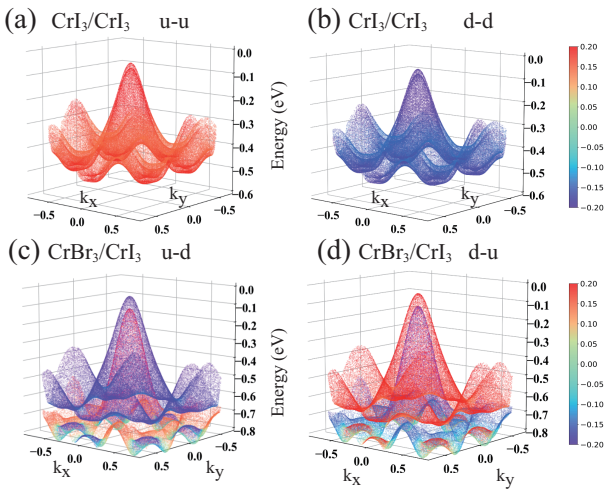

Figure 5: Spin texture of bands 1 and 2 (see also Figure 4) for (a) the up-up (u-u) or (b) down-down (d-d) FM state of $(CrI_3)_2$ bilayer, and for (c) the up-down (u-d) or (d) down-up (d-u) AFM state of $(CrBr_3/CrI_3)$. The color maps refer to the $\langle \hat{S}_z \rangle$ values. Note that the switching of Kerr rotation as discussed in the main text corresponds to the switching of red/blue colors of the corresponding bands involved in the optical excitations.

considering the level excitations associated with the left and right circularly polarized lights, their difference will give the MOKE signal in the (0,+M) FM $(CrI_3)_2$ bilayer. Moreover, it is evident that when we consider the (0,–M) FM $(CrI_3)_2$ bilayer, the $\hat{l}_z$ and $\hat{s}_z$ in Figure 4(f) just change to their opposite values — see Figure 4(g) and Figure 5(b), therefore giving a reversed MOKE signal compared with the (0,+M) FM state. Furthermore, for the (+L,0) (or (–L,0)) AFM $(CrI_3)_2$ bilayer (Figure 4(b)), bands 1 and 2 become degenerate (but with the opposite spins), and 'up' monolayer corresponds to Figure 4(f), and 'down' to Figure 4(g). Therefore, the net MOKE signal becomes exactly zero.

In the (+L,0) AFM $(CrBr_3/CrI_3)$ bilayer (Figure 4(c)), the Br $4p$ bands lie lower than the I $5p$ bands (Figure 4(e)). As a result, the two topmost valence bands 1 and 2 (I $5p$ ones in the spin-down CrI_3 monolayer) are now the two levels in Figure 4(g), down-spin $|1,-1\rangle$ and up-spin $|1,+1\rangle$ (see Figure 5(c)) . The spin-down CrI_3 and spin-up $CrBr_3$ monolayers would yield MOKE signals of opposite sign, but arising from transitions at different energy (lower Br $4p$ levels, smaller SOC, weaker spin polarization and smaller exchange splitting for $CrBr_3$). This explains why the AFM $(CrBr_3/CrI_3)$ bilayer shows a much reduced but non-

vanishing MOKE signal. Naturally, the (–L,0) AFM ($CrBr_3/CrI_3$) mixed bilayer (Figure 4(d) and Figure 5(d)) gives a reversed MOKE signal, compared with the (+L,0) one. Then the unusual MOKE signal in the AFM ($CrBr_3/CrI_3$) bilayer can also be reversed. In this respect, the AFM ($CrBr_3/CrI_3$) bilayer represents an interesting candidate for AFM spintronics: by initializing the bilayer in the time-reversed (+L,0) or (–L,0) states, magnetic information can be stored and read optically by MOKE. We foresee possible applications using mixed magnetic bilayers AFM memory elements.

4 Conclusion

We have studied the MOKE spectra of $(CrI_3)_2$ bilayer and ($CrBr_3/CrI_3$) mixed bilayer in four different (0, ±M) and (±L, 0) magnetic states, using symmetry analyses and first-principles calculations. Our arguments and results show that, for these emerging 2D materials, MOKE spectra (line shape and/or intensity) are very useful tools to identify different magnetic states, which are often correlated with different stacking of the monolayers. In particular, for the mixed bilayer even the AFM state has a non-vanishing MOKE signal, which can be reversed if the AFM spins are flipped (*e.g.*, from up-down to down-up). This singles out MOKE as a unique tool to study the magneto-optical properties of AFM bilayers in particular and related classes of AFM materials in general, and foreshadows its use a sensitive probe for the emerging field of AFM spintronics. Furthermore, the two time-reversed AFM states of the mixed bilayer could be used as memory element, since they show opposite Kerr rotation.

Acknowledgement

K. Y., W. H. and H. W. were supported by the NSF of China (Grants No. 11674064 and No. 11474059) and by the National Key Research and Development Program of China (Grant No. 2016YFA0300700). K.Y. and H.W. kindly acknowledge the hospitality of CNR-SPIN c/o Department of Physical and Chemical Science at University of L'Aquila (Italy) during

their visiting stay. A.S. would like to thank Oxford University (UK) for kind hospitality during his visit.

Supporting Information Available

SI. Selection Rules and SII. Symmetry-adapted form of the optical conductivity tensor σ_{ij} for all the magnetic point groups

References

(1) Huang, B.; Clark, G.; Navarro-Moratalla, E.; Klein, D. R.; Cheng, R.; Seyler, K. L.; Zhong, D.; Schmidgall, E.; McGuire, M. A.; Cobden, D. H.; Yao, W.; Xiao, D.; Jarillo-Herrero, P.; Xu, X. Layer-dependent ferromagnetism in a van der Waals crystal down to the monolayer limit. *Nature* **2017**, *546*, 270.

(2) Gong, C.; Li, L.; Li, Z.; Ji, H.; Stern, A.; Xia, Y.; Cao, T.; Bao, W.; Wang, C.; Wang, Y.; Qiu, Z. Q.; Cava, R. J.; Louie, S. G.; Xia, J.; Zhang, X. Discovery of intrinsic ferromagnetism in two-dimensional van der Waals crystals. *Nature* **2017**, *546*, 265.

(3) Burch, K. S.; Mandrus, D.; Park, J.-G. Magnetism in two-dimensional van der Waals materials. *Nature* **2018**, *563*, 47.

(4) Deng, Y.; Yu, Y.; Song, Y.; Zhang, J.; Wang, N. Z.; Sun, Z.; Yi, Y.; Wu, Y. Z.; Wu, S.; Zhu, J.; Wang, J.; Chen, X. H.; Zhang, Y. Gate-tunable room-temperature ferromagnetism in two-dimensional Fe_3GeTe_2. *Nature* **2018**, *563*, 94.

(5) Bonilla, M.; Kolekar, S.; Ma, Y.; Diaz, H. C.; Kalappattil, V.; Das, R.; Eggers, T.; Gutierrez, H. R.; Phan, M.-H.; Batzill, M. Strong room-temperature ferromagnetism in VSe_2 monolayers on van der Waals substrates. *Nat. Nanotechnol.* **2018**, *13*, 289.

(6) Yu, W.; Li, J.; Herng, T. S.; Wang, Z.; Zhao, X.; Chi, X.; Fu, W.; Abdelwahab, I.; Zhou, J.; Dan, J.; Chen, Z.; Chen, Z.; Li, Z.; Lu, J.; Pennycook, S. J.; Feng, Y. P.; Ding, J.; Loh, K. P. Chemically Exfoliated VSe_2 Monolayers with Room-Temperature Ferromagnetism. *Adv. Mater.* **2019**, *0*, 1903779.

(7) Zhang, Z.; Shang, J.; Jiang, C.; Rasmita, A.; Gao, W.; Yu, T. Direct photoluminescence probing of ferromagnetism in monolayer two-dimensional $CrBr_3$. *Nano Lett.* **2019**, *19*, 3138–3142.

(8) Huang, B.; Clark, G.; Klein, D. R.; MacNeill, D.; Navarro-Moratalla, E.; Seyler, K. L.; Wilson, N.; McGuire, M. A.; Cobden, D. H.; Xiao, D.; Yao, W.; Jarillo-Herrero, P.; Xu, X. Electrical control of 2D magnetism in bilayer CrI_3. *Nat. Nanotechnol.* **2018**, *13*, 544.

(9) Abramchuk, M.; Jaszewski, S.; Metz, K. R.; Osterhoudt, G. B.; Wang, Y.; Burch, K. S.; Tafti, F. F. Controlling magnetic and optical properties of the van der Waals crystal $CrCl_{3-x}Br_x$ via mixed halide chemistry. *Adv. Mater.* **2018**, *30*, 1801325.

(10) Kazim, S.; Ali, M.; Palleschi, S.; D'Olimpio, G.; Mastrippolito, D.; Politano, A.; Gunnella, R.; Cicco, A. D.; Renzelli, M.; Moccia, G.; Cacioppo, O. A.; Alfonsetti, R.; Strychalska-Nowak, J.; Klimczuk, T.; Cava, R.; Ottaviano, L. Mechanical exfoliation and layer number identification of single crystal monoclinic $CrCl_3$. *Nanotechnology* **2020**, *in press*, http://iopscience.iop.org/10.1088/1361–6528/ab7de6.

(11) Cai, X.; Song, T.; Wilson, N. P.; Clark, G.; He, M.; Zhang, X.; Taniguchi, T.; Watanabe, K.; Yao, W.; Xiao, D.; McGuire, M. A.; Cobden, D. H.; Xu, X. Atomically Thin $CrCl_3$: An in-Plane Layered Antiferromagnetic Insulator. *Nano Lett.* **2019**, *19*, 3993.

(12) Jiang, S.; Shan, J.; Mak, K. F. Electric-field switching of two-dimensional van der Waals magnets. *Nat. Mater.* **2018**, *17*, 406.

(13) Sivadas, N.; Okamoto, S.; Xu, X.; Fennie, C. J.; Xiao, D. Stacking-dependent magnetism in bilayer CrI_3. *Nano Lett.* **2018**, *18*, 7658.

(14) Jang, S. W.; Jeong, M. Y.; Yoon, H.; Ryee, S.; Han, M. J. Microscopic understanding of magnetic interactions in bilayer CrI_3. *Phys. Rev. Mater.* **2019**, *3*, 031001.

(15) Sun, Z.; Yi, Y.; Song, T.; Clark, G.; Huang, B.; Shan, Y.; Wu, S.; Huang, D.; Gao, C.; Chen, Z.; McGuire, M.; Cao, T.; Xiao, D.; Liu, W.; Yao, W.; Xu, X.; Wu, S. Giant nonreciprocal second-harmonic generation from antiferromagnetic bilayer CrI_3. *Nature* **2019**, *572*, 497.

(16) Jiang, P.; Wang, C.; Chen, D.; Zhong, Z.; Yuan, Z.; Lu, Z.-Y.; Ji, W. Stacking tunable interlayer magnetism in bilayer CrI_3. *Phys. Rev. B* **2019**, *99*, 144401.

(17) Song, T.; Cai, X.; Tu, M. W.; Zhang, X.; Huang, B.; Wilson, N. P.; Seyler, K. L.; Zhu, L.; Taniguchi, T.; Watanabe, K.; McGuire, M. A.; Cobden, D. H.; Xiao, D.; Yao, W.; Xu, X. Giant tunneling magnetoresistance in spin-filter van der Waals heterostructures. *Science* **2018**, *360*, 1214.

(18) Gibertini, M.; Koperski, M.; Morpurgo, A. F.; Novoselov, K. S. Magnetic 2D materials and heterostructures. *Nat. Nanotechnol.* **2019**, *14*, 408.

(19) Jungwirth, T.; Marti, X.; Wadley, P.; Wunderlich, J. Antiferromagnetic spintronics. *Nat. Nanotechnol.* **2016**, *11*, 231.

(20) Marrows, C. H. Addressing an antiferromagnetic memory. *Science* **2016**, *351*, 558.

(21) Liu, Z.; Feng, Z.; Yan, H.; Wang, X.; Zhou, X.; Qin, P.; Guo, H.; Yu, R.; Jiang, C. Antiferromagnetic piezospintronics. *Adv. Electron. Mater.* **2019**, 1900176.

(22) Godinho, J.; Reichlová, H.; Kriegner, D.; Novák, V.; Olejník, K.; Kašpar, Z.; Šobáň, Z.; Wadley, P.; Campion, R.; Otxoa, R.; Roy, P. E.; elezný, J.; Jungwirth, T.; Wunder-

lich, J. Electrically induced and detected Néel vector reversal in a collinear antiferromagnet. *Nat. Commun.* **2018**, *9*, 4686.

(23) Wadley, P.; Howells, B.; Železný, J.; Andrews, C.; Hills, V.; Campion, R. P.; Novák, V.; Olejník, K.; Maccherozzi, F.; Dhesi, S. S.; Martin, S. Y.; Wagner, T.; Wunderlich, J.; Freimuth, F.; Mokrousov, Y.; Kuneš, J.; Chauhan, J. S.; Grzybowski, M. J.; Rushforth, A. W.; Edmonds, K. W.; Gallagher, B. L.; Jungwirth, T. Electrical switching of an antiferromagnet. *Science* **2016**, *351*, 587.

(24) Park, B.; Wunderlich, J.; Marti, X.; Holý, V.; Kurosaki, Y.; Yamada, M.; Yamamoto, H.; Nishide, A.; Hayakawa, J.; Takahashi, H.; Shick, A. B.; Jungwirth, T. A spin-valve-like magnetoresistance of an antiferromagnet-based tunnel junction. *Nat. Mater.* **2011**, *10*, 347.

(25) Higo, T.; Man, H.; Gopman, D. B.; Wu, L.; Koretsune, T.; Erve, O. V. T.; Kabanov, Y. P.; Rees, D.; Li, Y.; Suzuki, M.; Patankar, S.; Ikhlas, M.; Chien, C. L.; Arita, R.; Shull, R. D.; Orenstein, J.; Nakatsuji, S. Large magneto-optical Kerr effect and imaging of magnetic octupole domains in an antiferromagnetic metal. *Nat. Photonics* **2018**, *12*, 73.

(26) Polisetty, S.; Scheffler, J.; Sahoo, S.; Wang, Y.; Mukherjee, T.; He, X.; Binek, C. Optimization of magneto-optical Kerr setup: Analyzing experimental assemblies using Jones matrix formalism. *Rev. Sci. Instrum.* **2008**, *79*, 055107.

(27) Aroyo, M. I.; Perez-Mato, J.; Orobengoa, D.; Tasci, E.; De La Flor, G.; Kirov, A. Crystallography online: Bilbao crystallographic server. *Bulg. Chem. Commun* **2011**, *43*, 183.

(28) Neumann, F. *Vorlesungen über die Theorie der elastischen, der festen Körper und das Lichtathers*; 1885.

(29) Sivadas, N.; Okamoto, S.; Xiao, D. Gate-controllable magneto-optic Kerr effect in layered collinear antiferromagnets. *Phys. Rev. Lett.* **2016**, *117*, 267203.

(30) Feng, W.; Guo, G. Y.; Zhou, J.; Yao, Y.; Niu, Q. Large magneto-optical Kerr effect in noncollinear antiferromagnets Mn_3X(X= Rh, Ir, Pt). *Phys. Rev. B* **2015**, *92*, 144426.

(31) Feng, W.; Guo, G.-Y.; Yao, Y. Tunable magneto-optical effects in hole-doped group-IIIA metal-monochalcogenide monolayers. *2D Mater.* **2016**, *4*, 015017.

(32) Yao, Y.; Kleinman, L.; Macdonald, A. H.; Sinova, J.; Jungwirth, T.; Wang, D.; Wang, E.; Niu, Q. First principles calculation of anomalous Hall conductivity in ferromagnetic bcc Fe. *Phys. Rev. Lett.* **2004**, *92*, 037204.

(33) Ebert, H. Magneto-optical effects in transition metal systems. *Rep. Prog. Phys.* **1996**, *59*, 1665.

(34) Oppeneer, P. Magneto-optical Kerr spectra. *Handb. Magn. Mater.* **2001**, *13*, 229.

(35) Zhou, X.; Hanke, J.-P.; Feng, W.; Li, F.; Guo, G.-Y.; Yao, Y.; Blügel, S.; Mokrousov, Y. Spin-order dependent anomalous Hall effect and magneto-optical effect in the noncollinear antiferromagnets Mn_3XN with X = Ga, Zn, Ag, or Ni. *Phys. Rev. B* **2019**, *99*, 104428.

(36) Feng, W.; Hanke, J.-P.; Zhou, X.; Guo, G.-Y.; Blügel, S.; Mokrousov, Y.; Yao, Y. Topological magneto-optical effects and their quantization in noncoplanar antiferromagnets. *Nat. Commun.* **2020**, *11*, 118.

(37) Fan, F.; Wu, H.; Nabok, D.; Hu, S.; Ren, W.; Draxl, C.; Stroppa, A. Electric-Magneto-Optical Kerr effect in a hybrid organic–inorganic perovskite. *J. Am. Chem. Soc.* **2017**, *139*, 12883.

(38) McGuire, M. A.; Dixit, H.; Cooper, V. R.; Sales, B. C. Coupling of crystal structure

and magnetism in the layered, ferromagnetic insulator CrI_3. *Chem. Mater.* **2015**, *27*, 612.

(39) Gallego, S. V.; Etxebarria, J.; Elcoro, L.; Tasci, E. S.; Perezmato, J. M. Automatic calculation of symmetry-adapted tensors in magnetic and non-magnetic materials: a new tool of the Bilbao Crystallographic Server. *Acta Crystallogr., Sect. A: Found. Adv.* **2019**, *75*, 438.

(40) Kresse, G.; Furthmüller, J. Efficient iterative schemes for ab initio total-energy calculations using a plane-wave basis set. *Phys. Rev. B* **1996**, *54*, 11169.

(41) Kresse, G.; Joubert, D. From ultrasoft pseudopotentials to the projector augmented-wave method. *Phys. Rev. B* **1999**, *59*, 1758.

(42) Perdew, J. P.; Burke, K.; Ernzerhof, M. Generalized gradient approximation made simple. *Phys. Rev. Lett.* **1996**, *77*, 3865.

(43) Huang, C.; Feng, J.; Wu, F.; Ahmed, D.; Huang, B.; Xiang, H.; Deng, K.; Kan, E. Toward Intrinsic Room-Temperature Ferromagnetism in Two-Dimensional Semiconductors. *J. Am. Chem. Soc.* **2018**, *140*, 11519.

(44) Liechtenstein, A.; Anisimov, V.; Zaanen, J. Density-functional theory and strong interactions: Orbital ordering in Mott-Hubbard insulators. *Physical Review B* **1995**, *52*, R5467.

(45) Togo, A.; Tanaka, I. First principles phonon calculations in materials science. *Scr. Mater.* **2015**, *108*, 1.

(46) Gulans, A.; Kontur, S.; Meisenbichler, C.; Nabok, D.; Pavone, P.; Rigamonti, S.; Sagmeister, S.; Werner, U.; Draxl, C. Exciting: a full-potential all-electron package implementing density-functional theory and many-body perturbation theory. *J. Phys.: Condens. Matter* **2014**, *26*, 363202.

(47) Singh, D. J.; Nordstrom, L. *Planewaves, Pseudopotentials, and the LAPW method*; Springer Science & Business Media, 2006.

(48) Alkauskas, A.; Schneider, S.; Sagmeister, S.; Ambrosch-Draxl, C.; Hébert, C. Theoretical analysis of the momentum-dependent loss function of bulk A_g. *Ultramicroscopy* **2010**, *110*, 1081.

TOC Graphic

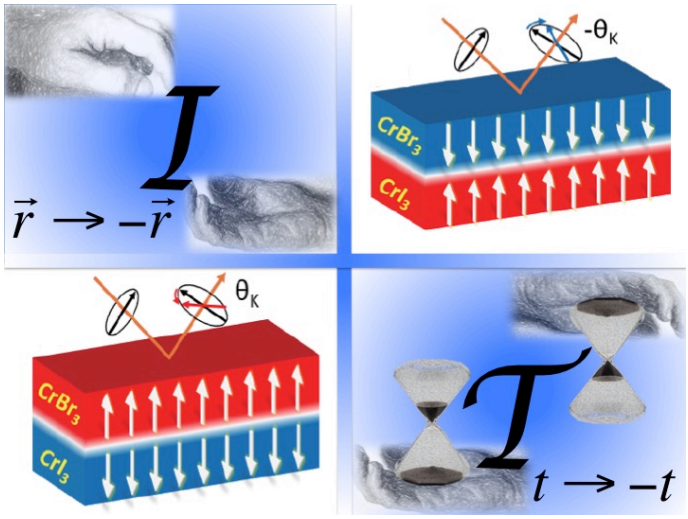
I
$\vec{r} \rightarrow -\vec{r}$
-θK
CrBr3
CrI3
θK
CrBr3
CrI3
T
$t \rightarrow -t$